UC San Diego

UC San Diego Previously Published Works

Title

ECH effects on toroidal rotation: KSTAR experiments, intrinsic torque modelling and gyrokinetic stability analyses

Permalink

https://escholarship.org/uc/item/3k96p2q1

Journal

Nuclear Fusion, 53(11)

ISSN

0029-5515

Authors

Shi, YJ
Ko, WH
Kwon, JM
et al.

Publication Date

2013-11-01

DOI

10.1088/0029-5515/53/11/113031

Copyright Information

This work is made available under the terms of a Creative Commons Attribution-NonCommercial-NoDerivatives License, availalbe at https://creativecommons.org/licenses/by-nc-nd/4.0/

Peer reviewed

eScholarship.org Powered by the California Digital Library
University of California

ECH Effects on Toroidal Rotation: KSTAR Experiments, Intrinsic Torque Modeling and Gyrokinetic Stability Analyses

[a,b]Y.J. Shi, [b]W.H. Ko, [a]J.M. Kwon, [a,c]P.H. Diamond, [b]S.G. Lee, [a]S. H. Ko, [d]L. Wang, [a]S. Yi, [e]K. Ida, [b]L. Terzolo, [b]S.W. Yoon, [b]K.D. Lee, [b]J.H. Lee, [b]U.N. Nam, [b]Y.S. Bae, [b]Y.K.Oh, [b]J.G.Kwak, [f]M. Bitter, [f]K. Hill [g]O. D. Gurcan, [h]T.S. Hahm

[a]WCI Center for Fusion Theory, National Fusion Research Institute, Daejeon 305-333, Korea
[b]KSTAR, National Fusion Research Insititute, Daejeon 305-333, Korea
[c]CMTFO and CASS, Universituy of California, San Diego, California 92904, USA
[d]Huazhong University of Science and Technology, Wuhan 430074, China
[e]National Institute for Fusion Science, Toki, GiFu 509-5292, Japan
[f]Princeton Plasma Physics Laboratory, Princeton, New Jesse 08543-0451, USA
[g]Ecole Polytechnique, CNRS, Palaiseau Cedex 91128, France
[h]Seoul National University, Seoul 151-742, Korea
Email: yjshi@nfri.re.kr

Abstract: Torodial rotation profiles have been investigated in KSTAR H-mode plasma using combined auxiliary heating by co-neutral beam injection (NBI) and electron cyclotron resonance heating (ECH). The ion temperature and toroidal rotation are measured with x-ray imaging crystal spectroscopy (XICS) and charge exchange recombination spectroscopy (CES). H-mode plasma is achieved using co-current 1.3MW NBI, and a 0.35 MW ECH pulse is added to the flattop of H-mode. The core rotation profiles, which are centrally peaked in the pure NBI heating phase, flatten when ECH is injected, while the edge pedestal is unchanged. Dramatic decreases in the core toroidal rotation values ($\Delta V_{tor}/V_{tor} \sim -30\%$) are observed when on-axis ECH is added to H-mode. The experimental data shows that the decrease of core rotation velocity and its gradient are correlated with the increase of core electron temperature and its gradient, and also with the likely steepening of the density gradient. We thus explore the viability of a hypothesized ITG→TEM transition as the explanation of the observed counter-current flow induced by ECH. However, the results of linear microstability analyses using inferred profiles suggest that the TEM is excited only in the deep core, so the viability of the hypothesized explanation is not yet clear.

PACS numbers: 52.55Hc, 52.55Fa, 52.50.Sw, 52.50.Gj

1. Introduction

Flow and velocity shear are very important for stabilizing micro- and macro-instabilities in tokamak plasmas. Neutral beam injection (NBI) is generally used as the external momentum input source to produce and control plasma rotation in present day tokamaks. For ITER and future reactors, the input torque from NBI will be very low or nonexistent and cannot produce the needed rotation. As a result, there is a need to develop alternative or complementary methods for driving plasma rotation. Significant intrinsic rotation (without external momentum input) has been observed on many tokamaks [1], which suggests that it may be possible to reap the benefits of such self-generated flows in ITER and reactors.

Since the discovery of intrinsic rotation in the 1990s [2, 3], plasma rotation without external torque has been a topic of intense interest. While significant progress has been made, the driving mechanism is not fully understood. Theoretical models have been proposed to explain intrinsic rotation as due to a turbulence driven intrinsic torque [4-7]. Intrinsic torque is dynamic and variable – due to evolving turbulent Reynolds stresses. Momentum transport bifurcations and reversals have been observed in several experiments [8, 9]. The effects on toroidal rotation of ECH have being observed previously in CHS [10], DIII-D [11], JT-60U[12] and AUG[13,14]. The counter-current rotation increment or flattening of co-current rotation profile was confirmed in these ECH experiments. The proposed explanations vary considerably. The KSTAR results in this paper, though partly similar to some previous experiments, will be combined with gyrokinetic stability analyses to elucidate possible physics mechanisms for ECH rotation experiments. In KSTAR H-mode, a core counter-current flow develops when ECH is injected. The pedestal is unchanged. KSTAR results suggest that toroidal rotation profiles in H-mode are determined by the interplay of i) a core co-current NBI torque, ii) a pedestal intrinsic torque, which is co-current, iii) a core intrinsic torque, which becomes counter-current with the addition of ECH(Pat mention to document this,how to do it?). Here, we investigate the hypothesis that the appearance of the core counter-current intrinsic torque with ECH is due to a transition from a state of ITG turbulence to a state of TEM turbulence, and thus a change in the sign of the turbulence-driven residual stress [4, 7]. This mechanism is very similar to that invoked for explaining the phenomenon of OH rotation direction reversals, where an increase in density triggers a confinement transition (LOC→SOC), the transition from TEM to ITG, and thus a change in sign of the predicted residual stress. In the core plasma of KSTAR, the ITG → TEM transition might be triggered by the steepening of ∇T_e, the peaking of ∇n_e, and the drop in ν_{e*} due to the addition of ECH. The key role of ∇n_e evolution highlights the point that particle and momentum transport are

strongly coupled.

This paper is organized as follows: an introduction to the experiment setup in KSTAR is given in section 2, which presents heating schemes, diagnostics and relevant plasma parameters. The main experimental results are described in section 3. Section 4 gives the analysis and interpretation of the effect of on-axis ECH heating plasma on toroidal rotation profiles in H-mode plasma. Conclusions and future plans are summarized in section 5.

2. Experimental setup

All the experimental results presented in this paper were obtained in the KSTAR superconducting tokamak [15]. Two diagnostics on KSTAR can measure the impurity ion rotation, temperature and brightness profiles. One is the x-ray imaging crystal spectroscopy (XICS) [16], which is a passive diagnostic and can provide nearly full-time information for all discharges using argon gas-puffing. The limitation of XICS in KSTAR is that only the core plasma is covered by XICS. The other diagnostic is the charge exchange recombination spectroscopy (CES) [17], which has 32 toroidal lines of sight and can provide the whole plasma profile from the plasma edge to the magnetic axis. CES in KSTAR needs NBI modulation to subtract the background signal and so CES can provide data for only a limited range of time. The temporal performance of XICS and full-spatial capacity of CES are *complementary* to each other. For the discharges where both XICS and CES can obtain data, there is good agreement of the core rotation velocity profiles from the two diagnostics. Thus, the rotation data presented here combines the results of XICS and CES. Electron temperature was measured with an electron cyclotron emission radiometer (ECE) [18].The line averaged density measurements are based on micro-wave interferometry and thus give indications of only the line averaged values. Thompson scattering data is not yet available.

The main plasma parameters in this paper are I_p = 0.6MA, B_T=2T. Discharges were operated in double or quasi-double null configuration. The plasma elongation factor is about 1.8~1.9. NBI is the main heating power in KSTAR. On-axis 1.2~1.4 MW NBI (90~95keV) [19] were always injected in the co-current direction during the flap-top in the discharges presented here. There are two ECH heating system in KSTAR [20]. One is 110GHz (source power 0.5MW) and the other is 170GHz (source power 1MW). The ECH system was configured for X-mode second harmonic @ 110GHz or third harmonic @ 170GHz and deposition location was set using steerable mirrors. The toroidal angle of ECH is almost perpendicular to the magnetic field such that the current driven effect can be neglected.

3. Experimental results

One typical set of waveforms for combined auxiliary heating of NBI and ECH is shown in Figure.1. 1.3MW NBI was injected from 1.0s to 7.0s and was sustained during the major part of the discharge pulse. H-mode plasma was achieved from 2.1 s and sustained to 6.5s by NBI, which is clearly indicated by the increment of stored energy and the D_α ELM signal. The center line averaged density was about $2.5\times10^{19}m^{-3}$ before L-H transition and increased to $3.4\times10^{19}m^{-3}$ after L-H transition. The core rotation also increased by about 80 km/s after the L-H transition. A 0.5s duration pulse of 350 kW on-axis ECH was added in the steady-state phase of H-mode plasma. Many parameters responded to the injection of ECH. The core electron temperature and its gradient increased significantly due to the direct heating by ECH. Plasma stored energy also increased about 13%. The core ion temperature decreased slightly (about 11%). At the same time, the core toroidal rotation dramatically decreased by 30%. Figure 2 shows the rotation profile for NBI phase and ECH phase from XICS and CES. The results from each of the two diagnostics clearly show the peaked rotation profiles in NBI phase evolve to flat profiles after injection of ECH. Note the region of change, i.e.$\rho< \rho_{pv}$ where ρ_{pv} is the point about which the profile pivots in Fig 2a, clearly lies within the core, and dose not overlap the pedestal (i.e. $\rho_{pv}< \rho_{ped}$, where ρ_{ped} is the position of the top of the pedestal). The pedestal rotation is unchanged. Figure 2d shows the detailed time traces of rotation velocity at different positions during the ECH phase, which show that the response of core rotation to ECH is faster than that of the rotation elsewhere. The significant decrease in core rotation cannot be explained by degradation of momentum confinement [13] and the slight decrease of ion pressure gradient or by a change in the beam torque. From figure 1 and figure 2, we see that the change in rotation is correlated with the increase in the electron temperature gradient.

Figure 3 shows the results for different waveforms of on-axis ECH and NBI heating. 110GHz ECH was injected at startup and flat-top in the L-mode phase. At 1.8s, a 170GHz ECH pulse covered both L-mode and H-mode phases in this shot. After the injection of ECH, the core temperature and stored energy increased. The toroidal rotation dropped markedly in both the 110GHz ECH L-mode phase and 170GHz ECH L-mode phase. Although, the power of the 170GHz ECH is much higher than of the 110GHz ECH, the decrease of rotation velocity was almost the same for the two heating phases. The reason is likely that the heating efficiency of 170GHz EC waves at third harmonic is much lower than that of 110GHz EC waves at 2nd

harmonic. The increment of core rotation $\Delta V(r) = V_H(r) - V_L(r)$ due to the L-H transition in this discharge is much lower than for the pure NBI induced H-mode plasma in figure.1 (The profiles of the increment for the two cases are shown in fig 4a). It can be seen that the increment in rotation is almost the same in the outer plasma, while the core rotation increment for pure NBI achieved in H-mode is much higher than that with ECH injection. The peaked increment profile of rotation in figure4 is caused mainly by the co-current intrinsic torque driven by the H-mode pedestal. When ECH is injected during H-mode, the core counter-current intrinsic torque opposes the effect of the pedestal co-current intrinsic torque. The flat increment profile in figure 4a is then the result of the balance between the two torques. On the other hand, rotation decreases over a broad spatial range when ECH is injected into an L-mode plasma (as shown in fig4b). A likely reason is that the effects of the counter-current torque can easily spread to larger radii without opposition from a pedestal intrinsic torque. The comparison between rotation profiles for two kinds of L-H transition (with ECH and without ECH during L-H) and L-mode and H-mode ECH plasma demonstrate that the rotation profiles for ECH+NBI H-mode plasma are determined by the three way competition between the core co-NBI torque, the pedestal intrinsic co-torque, and the core ECH-induced counter torque.

Considerable insight may be gleaned by consideration of macroscopic correlations. Of course, these are only *correlations* and do not establish *causality*. The first pair of plots in figure 5 shows a plot of $-\Delta V_\phi$ (change in V_ϕ due to ECH) vs ΔT_e, the change in the central electron temperature. A linear scaling relation is apparent. Note that this is the ECH analogue of a 'Rice scaling' ($\Delta V_\phi \sim \Delta W/I_p$) and gives the relation between the increment of *reduction* in V_ϕ and the increase in electron temperature. The second pair of figures in Fig. 5 show the correlation between the change in $-dT_e/dr$ (i.e. compare NBI points with NBI+ECH points) and dV_ϕ/dr The trend showing that steepening of dT_e/dr is accompanied by a reduction in dV_ϕ/dr is apparent. Just as the first pair of figures was the ECH analogue of the *macroscopic* Rice scaling, this pair is the analogue of previous *local* intrinsic rotation studies which showed the correlation between $V_\phi(0)$ and pedestal dT_i/dr [21, 22]. The third pair of plots in Fig. 5 shows the change (NBI vs NBI+ECH) in dV_ϕ/dr vs dT_i/dr. In this case, the scatter is larger. Still, the data indicates that the *flattening* of dV_ϕ/dr is accompanied by a *reduction* in dT_i/dr along with an *increase* in dT_e/dr. This suggests that the appearance of the ECH-induced counter-torque is accompanied by a change in the species which stores the

preponderance of free energy. All told, Fig.5 strongly suggests that the ECH-induced counter-intrinsic torque is ∇T_e driven.

The correlation of $\Delta\nabla V_\phi$ with $\Delta\nabla T_e$, and our cognizance of the theoretical prediction that a change in mode propagation direction can change the sign of the residual stress Π^R and hence that of the intrinsic torque density $\tau = -\partial_r \Pi^R$, lead us to investigate other ECH-induced changes which may signal a tip of the system toward the electron channel. Fig.6b shows the collision frequency plotted vs. ρ for NBI-only and NBI+ECH. Rather clearly, ECH triggers a drop in ν_{*e} by a factor 2~3. In the NBI+ECH cases, electron collisions are still non-negligible, but trapped electron modes are surely possible. As the trapped electron mode frequency and growth depend heavily on ∇n, we should also look for a density profile change with ECH. No core density profile information is available for KSTAR. We found the line averaged density always increases slightly when on-axis ECH is injected in KSTAR. Moreover, the profile of Argon radiation measure with XICS becomes more peaked during the injection of ECH (as shown in Fig.6). Indications from measurements of line averaged density are that some ∇n peaking occurs, as in similar experiments elsewhere [13]. Based on the line averaged data and impurity profiles, we have constructed a range of possible "synthetic" n(r) profiles which are shown in Fig.7a.

4. Analysis and Interpretation

The drop in collisionality, the steepening of ∇T_e and slight drop in ∇T_i, the indirect evidence that ∇n steepens, and the correlation of $\Delta\nabla V_\phi$ with $\Delta\nabla T_e$ as NBI → NBI+ECH all together suggest the hypothesis *that a TEM driven core counter-torque acts to modify the KSTAR rotation profiles*. Noting that theory and simulation predict that residual stress can change sign as the turbulence flips from ITG→TEM (i.e. $V_{*i} \rightarrow V_{*e}$, so the direction of V_{gr} changes) and that ∇T_e can drive a residual stress via TEM [23], we now investigate the evidence for a change in the direction of the turbulence driven torque. Three issues arise – first, the dynamics of ∇n peaking must be understood. This is important since ∇n steepening reduces η_i and so works against ITG and for TEM. More generally, this tells us that the particle and momentum channels are strongly coupled. Second - the mechanism of symmetry breaking in the TEM residual stress must be identified. Electric field shear is quite modest in the core of KSTAR, so the viability of the conventionally invoked mechanism is unclear. Third - is there actual quantitative evidence for the change in character of the underlying micro-turbulence? We address these issues here. Regarding the first, the unavailability of density profile information

makes any substantive work impossible. Similarly, without an $n_e(r)$ profile, no progress on impurity profile effects is possible. Thus, we are limited only to exploring a range of synthetic density profiles. We remark here that the phenomenon of density peaking in ECH+NBI is not easily reconciled with a change in the mode population from ITG→TEM, since TEM produces outward convection (i.e. thermoelectric piece beats the inward TEP pinch) so that 'density pump out' is predicted. Our stability analysis suggests that mode frequencies are not low enough to fall in the murky transition region, so that the escape route between ITG and TEM is not available. Beam related effects are a possibility, but we cannot offer a satisfactory explanation at this point. Regarding the second, direct measurement of the structure of the residual stress is not possible, except by HIBP or edge Langmuir probes. Hence, we are limited to inferences based on indirect macroscopic evidence. Regarding the third, nonlinear gyrokinetic simulation of rotation profile evolution is beyond the capability of present day codes. Thus, we perform linear gyrokinetic stability analysis of experimentally determined profiles, so as to compare results for NBI-only plasmas (i.e. "before") with NBI+ECH (i.e. "after") plasmas. Results which address the second and third issues are presented below.

Here we address symmetry breaking and the structure of the residual stress. Regarding symmetry breaking, Fig. 6c shows a comparison of ExB velocity (V_E) profiles for NBI only and NBI+ECH cases. To obtain V_E, radial force balance is used, where $T_i(r)$ and $V_\phi(r)$ are measured, $n(r)$ is synthesized (though constrained by line averaged data) and $V_\theta(r)$ is calculated, assuming neoclassical rotation. Plots indicate that V_E actually *decreases* with ECH, due to the increase in n and the flattening of $V_\phi(r)$. V'_E is roughly constant. This outcome is in distinct contrast to the case of ETBs or ITBs, where the increase in intrinsic torque is accompanied by an *increase* in V'_E. In contrast, Fig.6d compares a plot of $1/L_{Te}$ 'before' and 'after'. Clearly, $1/L_{Te}$ *increases* with ECH. Now, we also note that L_{Te} is effectively an upper bound on the *turbulence intensity gradient scale*, set by the scale $L_I = (\partial_r I/I)^{-1}$, where I is the local fluctuation intensity. Recall that a finite intensity gradient *breaks spectral* $\langle k_\theta k_{||}\rangle$ *symmetry* by yielding a finite dispersion in $k_{||}$ [4, 24]. Thus, we see that the strength of symmetry breaking by intensity gradient actually *increases* with ECH, giving a positive feedback loop. This leads us to analyze the implications of that mechanism for ECH-induced intrinsic torque. A gyrokinetic calculation of the residual stress $\Pi^R_{r\phi}$ for CTEM turbulence gives the prediction that [25]:

$$\Pi^R_{r\phi} = 2\frac{\Omega_i}{L_I}\frac{\hat{s}}{Rq}\sum_{\underline{k}}\tau_{c\underline{k}}k_\theta^2\varrho_s^2c_s^2x^2\left|\frac{e\widehat{\phi}_k}{T_e}\right|^2\left(1+2\tau+4\tau^2\frac{L_n}{R_0}\right) \quad (1)$$

Here, $L_I^{-1} = (1/I)(\partial I/\partial r)$ is the intensity gradient scale length, $\tau = T_i/T_e$, $x = r - r_{0\,m,n}$ with $r_{0\,m,n}$ is the radial location of the resonance surface, and $\tau_{c\underline{k}}$ is the correlation time. We use the mixing length estimation for turbulence intensity, $I \sim (l_c/L_{T_e})^2$ with l_c is the correlation length, and so $1/L_I \sim 2/L_{T_e}$ is used in deriving Eq. (1) (we didn't assume $L_I \sim L_{T_e}$ diretly). The distinction between parallel and toroidal is ignored in Π^R. Then taking $L_I \sim L_{T_e} > 0$ ($L_{T_e} \equiv -(1/T_e)(\partial T_e/\partial r)$, using the mixing length estimate $I \sim (l_c/L_{T_e})^2$ so $1/L_I \sim 2/L_{T_e}$, performing the spectral sum, and balancing CTEM residual stress with diffusion give:

$$\Delta\left(\frac{\partial\langle v_\phi\rangle}{\partial r}\right) \cong 2\Omega_i \frac{\Delta^2}{L_{T_e}} \frac{\hat{s}}{Rq}\left(1 + 2\tau + 4\tau^2 \frac{L_n}{R_0}\right) \quad (2)$$

Δ is the radial spectral width. Eqn. (2) gives the change in $\partial\langle v_\phi\rangle/\partial r$ induced by CTEM intrinsic torque. Note $\Delta\left(\partial\langle v_\phi\rangle/\partial r\right) > 0$, consistent with the observed rotation profile flattening. In obtaining Eqn. (2), χ_ϕ in NBI + ECH was approximated as equal to χ_ϕ for NBI, only. Thus, the effect of the external torque dose not enter $\Delta\left(\partial\langle v_\phi\rangle/\partial r\right)$. In reality, the external torques from NBI for CTEM and ITG are comparable, but $\chi_\phi^{CTEM} \neq \chi_\phi^{ITG}$, so corrections should be considered. The key point concerning Eqn. (2) is that $\Delta\left(\partial\langle v_\phi\rangle/\partial r\right) \sim 1/L_{T_e}$, consistent with the results of the middle panel (XICS) in Fig. 5. Finally, keep in mind that necessarily $L_I < L_{T_e}$, so Eqn (2) gives a lower bound on the strength of the CTEM-induced counter torque.

Regarding the third issue in the above section, we analyzed the change in linear micro-instability caused by ECH injection using the flux tube gyrokinetic code GS2. We compared the linear stability of the plasma profiles for NBI only to those of the plasma profiles for NBI+ECH including electron and ion collisions, ExB shearing, and toroidal rotation. We used the ion temperature and rotation profiles measured by CES and the electron temperature profiles by ECE. Without any measured density profile, we synthesized one as follows. The density profile at the time with NBI only is assumed to take the form $n_e(\rho) = \left(n_e(0) - n_e(1)\right) \times (1-\rho^2)^{0.4} + n_e(1)$, $n_e(1) = 0.15 \times n_e(0)$. Here, ρ represents a radial coordinate defined as $\rho = \sqrt{\psi/\psi_x}$ for the poloidal magnetic flux ψ and ψ_x *is* the flux value at last closed flux surface. After ECH injection, the profile of Ar emissivity indicates moderate density peaking. As shown in figure 6a, two cases for density peaking during ECH injection are assumed. One is moderate peaking profile. The other is a sharp peaked profile. The profiles for ECH phase are assumed to be of the form $n_e(\rho) = n_{e1}(\rho) + n_{e2}(\rho)$, $n_{e1}(\rho) =$

$\left(n_{e1}(0) - n_{e1}(1)\right) \times (1-\rho^2)^{0.4} + n_{e1}(1)$, $n_{e2}(\rho) = n_{e2}(0) \times (1-(\rho/\rho_0)^2)^2, n_{e1}(1) = 0.19 \times n_{e1}(0)$, $n_{e2}(0) = 0.15 \times n_{e1}(0)$ (moderate density peaking) $n_{e1}(1) = 0.17 \times n_{e1}(0)$, $n_{e2}(0) = 0.47 \times n_{e1}(0)$(sharp density peaking) and $n_{e2}(\rho) = 0$ if $\rho \geq \rho_0$. The line averaged density values were used to find $n_e(0)$ and $n_{e1}(0)$. Based on the Ar emissivity profile, we chose $\rho_0 = 0.6$. Based on the observation that the toroidal rotation change occurs within $= \rho_p$, with $\rho_p = 0.7$ as a pivot point, we chose 3 different radial positions ($\rho = 0.18, 0.3, 0.5$) for the analysis of the variation of the dominant micro-instabilitiy growth.

Before ECH injection, the plasma profiles support Ion Temperature Gradient Modes (ITG) in the $\rho < 0.6$ region, as we can see in Fig.7 (green dots). First, let's focus on the moderate density peaking case. During ECH injection, Trapped Electron Modes (TEM) become unstable for high $k_\theta > 0.5$ in deep core ($\rho = 0.18$), due to relatively moderate density gradients (Fig.7 red dots). Note that negative frequencies here correspond to propagation in the electron diamagnetic direction. The increase in electron temperature and its steepened gradient lead to the excitation of TEM in the deep core ($\rho = 0.18$) after the ECH injection. We can see that for wave numbers $k_\theta > 0.5$, a change of micro-instabilities occurs i.e. ITG→TEM. In other regions, ECH injection causes little change - the dominant mode is still ITG, albeit with reduced frequencies and growth rates. When the density is more peaked (sharp peaking case in fig6a), it can be seen that the change of micro-instabilities occurs for the whole range of wave numbers at $\rho = 0.18$ and $\rho = 0.3$. Compared to the conservative density peaking case, the mode flip is clear the region. On the other hand, the range of excitation of TEM is still limited to deep core even for sharp peaking case. Thus, a problem emerges, namely that the popularly favored hypothesis is not supported by the data. To address this issue, we remark that fluctuation intensity can spread beyond the linearly unstable region by nonlinear scattering processes such as turbulence spreading and heat avalanches [26], etc. Thus, resolving the physical problem may require consideration of non-locality processes. Also, the limited extent of the region where the dominant micro-instability changes suggests that the state of turbulence in neighboring radial regions is very likely a dynamic, evolving mixture of both ITG and TEM turbulence. The ideas of mixed states of both TEM and ITG, and the extension of TEM influence with nonlinear processes are shown in the simple cartoon in figure 9. The intrinsic torque from this mixed population of ITG and TEM will be determined by the competition between different spectral components of the momentum flux, and may not be possible to calculate within a simple quasi-linear approach. Detailed study of this process requires global nonlinear simulation and more detailed

modeling, which are subjects for future work. We remark here that this rather unsatisfactory result dramatizes the need for accurate measurement of density and impurity profiles, and for spatially localized heterodyne fluctuation measurements in coordination with macroscopic profile studies.

5. Summary , discussion and future plans

ECH induces a counter-current rotation increment in the L-mode and H-mode co-NBI plasmas studied so far. Both XICS and CES confirm that the core toroidal rotation dramatically decreases when a modest amount of on-axis ECH is injected to H-mode plasmas. Both the change of rotation and its gradient have a close relation to the change of electron temperature and its gradient in the core plasma. However, analyses show that the popular, simple explanation of the intrinsic counter torque as a consequence of the turbulence 'flipping' from ITG→TEM is somewhat problematic. First, the symmetry breaking mechanism for the residual stress needs to be clarified. We offer intensity gradient as a relevant improvement over $\langle V_E \rangle'$, but further work is needed. Second, gyrokinetic micro-stability analysis using experimental profiles indicates that and region of mode flip transition is very sensitive to the density peaking. More peaked density profiles favorite a broader mode flip region. Third, the ITG→TEM flip is limited only to the deep core ($\rho < 0.2 \sim 0.3$), while the intrinsic torque has an impact for all $\rho \leq \rho_{piv} \sim 0.7$. Thus, certainly a mixed state will occur, and consideration of turbulence propagation or other type of non-local effect may be required. Density profile evolution is clearly critical to this study, and a satisfactory explanation of the peaking phenomenon is as yet elusive. Momentum and particle transport are coupled and must be studied together.

The other possible mechanism for the counter-current rotation induced by ECH is a neo-classical toroidal viscosity (NTV) effect [27]. Indeed, some weak n:m=1:1 kink mode appeared when ECH was injected in KSTAR 2011's campaign. For the ECH+NBI plasma in KSTAR, we don't think NTV is the main source of torque. There are two pieces of experiment evidence in KSTAR which don't support by the NTV hypothesis. One is the experimental results of off-axis ECH heating. The toroidal rotation still decreases when the resonance layer of ECH is far from the q~1 surface. The new ECH+NBI rotation results in 2012 show that there is no 1:1 kink mode in many discharges when ECH is injected to NBI plasma, but toroidal rotation still decreases.

Several lines for future work are apparent. For experiments, plans include:

i) scans with higher ECH power and a broader range of P_{ECH}/P_{NBI}. Comparisons with pure ECH cases become relevant as P_{ECH}/P_{NBI} increases.

ii) BES fluctuation studies, in coordination with macroscopics. Here, it is crucial to determine the centroid of the frequency spectrum in the local frame in order to address the ITG vs TEM issue. In addition, spatially well resolved fluctuation measurements could yield an intensity profile.

iii) exploration of counter-NBI H-modes + ECH, with the aim of exploring profile structure and the interaction of multiple torques. Note that a counter-NBI H-mode case should recover the Solomon experiment result of an approximate cancellation between counter-NBI + co-intrinsic pedestal torque. Then a natural question is whether adding ECH will expose the ECH counter-torque only, or whether something unexpected will occur. The ECH induced counter-current torque implied here could be compared to that obtained from analysis of the co-NBI cases. Comparative experiments on the interaction of multiple torques can be useful in revealing the rather nonlinear physics of rotation profile structure.

iv) coordinated experimental studies of particle transport.

v) comparison with OH reversals

In theory and computation, plans include:

i) further, much more comprehensive linear stability analysis of experimental profiles, including quantive calculation of Π^R.

ii) development of models of residual stress which incorporate turbulence spreading or propagation, to explore the effect of spatially limited domains of 'mode flip'. Likewise, theoretical approaches for understanding mixed states are being developed.

iii) nonlinear gyrofluid simulations of dynamically interacting domains and competing flux driven ITG and TEM turbulence. There are vital to address the key theoretical questions relevant to this problem.

iv) exploration of alternative scenarios

6. Acknowledgments

The authors thank the participants in the 24th IAEA FEC and 2th APTWG workshop for useful discussions and encouragement. This work was partly supported by the World Class Institute (WCI) Program of the National Research Foundation of Korea (NRF) funded by the Ministry of Education, Science and Technology of Korea (MEST) (NRF Grant No. WCI 2009-001) and US DOE.

Reference

[1] Rice J. E., et. al., Nucl. Fusion **47**, 1618 (2007);
[2] Ida K. et. al., Nucl. Fusion **31,** 943(1991);
[3] Rice J. E., et. al., et al., Nucl. Fusion **38,** 75(1998);
[4] Dimond P. H. et al., Phys. Plasmas **15**, 012303 (2008);
[5] Gurcan O. D., et. al., Phys. Plasmas **14**, 042306 (2007);
[6] Kwon J. M., et. al., Nucl. Fusion **52**, 013004 (2012);
[7] Camenen Y., et. al., Nucl. Fusion **51**, 073039 (2011);
[8] Bortolon A. et. al., Phy. Rev. Lett **97**, 235003 (2006);
[9] Rice J. E., et. al., Phy. Rev. Lett **107**, 265001 (2011);
[10] Ida K. et. al., Phy. Rev. Lett **86**, 3040 (2001);
[11] deGrassie J S et al., Phys. Plasmas **11**, 4323 (2004)
[12] Yoshida M et. al., Phy. Rev. Lett **103**, 065003 (2009);
[13] McDermott R. M., et. al., Plasma Phys. Control. Fusion **53,** 035007(2011);
[14] Angioni C., et. al., Phy. Rev. Lett **107**, 215003 (2011);
[15] Lee G. S., et. al., Nucl. Fusion **40**, 575 (2000);
[16] Lee S. G., et. al., Rev.Sci.Instrum. **81**, 10E506 (2010);
[17] Ko W. H., et. al., Rev.Sci.Instrum. **81**, 10D740 (2010);
[18] Jeong S. H., et. al., Rev.Sci.Instrum. **81**, 10D922 (2010);
[19] Bae Y. S., et. al., Fusion Enginerring and Design, in published;
[20] Bae Y. S., et. al., Status and near plan of KSTAR heating & CD devices, 2012 KSTAR conference (Muju, Korea, 2012);
[21] Ida K. et. al., Nucl. Fusion **50,** 064007(2010);
[22] Rice J. E., et. al., Phys.Rev. Lett. **106,** 215001(2011);
[23] Wang W. X.., et. al., Phys.Rev. Lett. **106,** 085001(2011);
[24] Gurcan O. D., et. al., Phys. Plasmas **17**, 032509 (2010);
[25]Wang L., et. al., "Parallel rotation profile in collisionless trapped electron mode turbulence", to be submitted
[26] Gurcan O.D., et. al., Phys. Plasmas 12, 032303 (2005)
[27] Shaing K. C. Shaing, Phys. Plasmas 10, 1443 (2003).

Figures

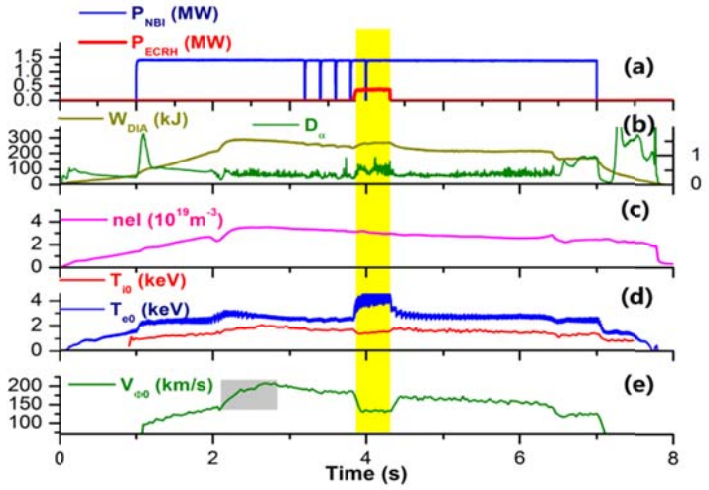

Figure 1. Time traces of main parameters for H-mode discharge (sn5737) on KSTAR. ECH is injected on the flattop of H-mode. (a) power of NBI and ECH, (b) stored energy W_{dia} and D_a intensity, (c) central line averaged density, (d) core electron and ion temperature, (e) core rotation velocity

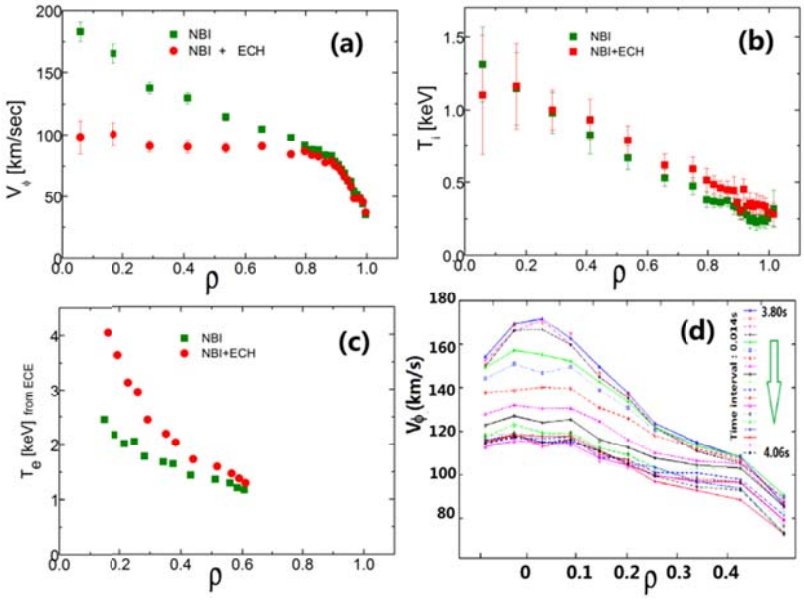

Figure 2.(a) profiles of rotation by CES,(b) ion temperature by CES, (c) electron temperature by ECE, (d)time evolution of rotation profiles by XICS(from 3.8s to 4.05s) during injection of ECH

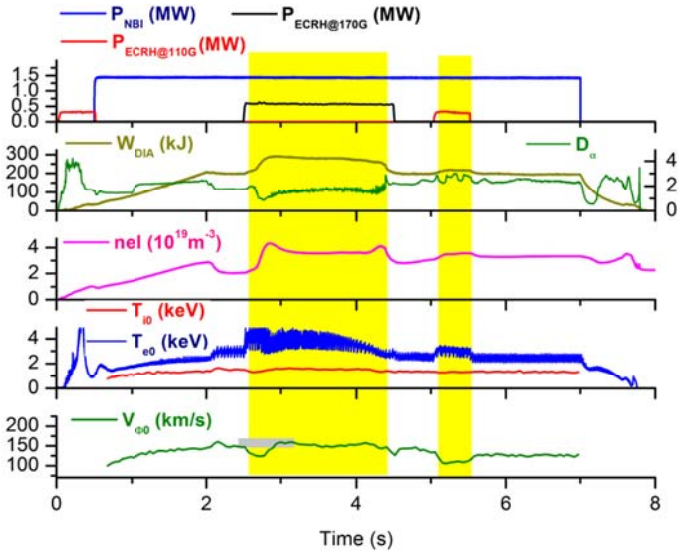

Figure 3. Time traces of main parameters for another H-mode discharge(sn6384). The signals are the same as those in figure 1.

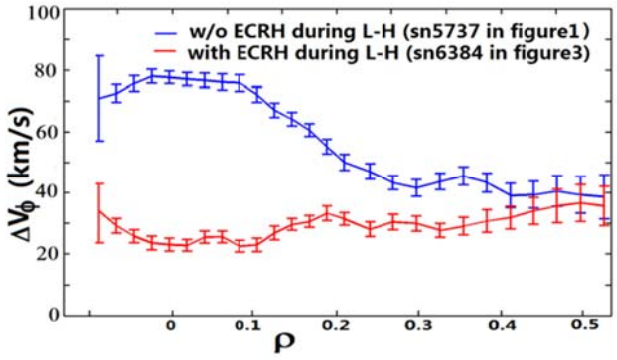

Figure4a. The profiles of rotation increment (measured with XICS)

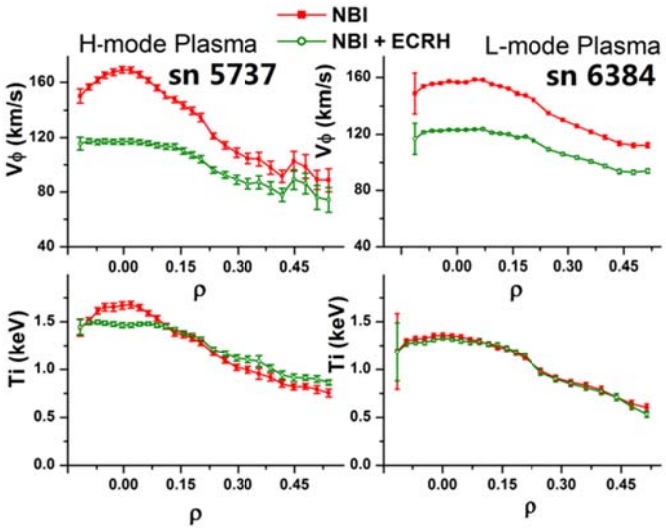

Figure4b. The profiles of rotation (up) and ion temperature (low) for two ECH cases.

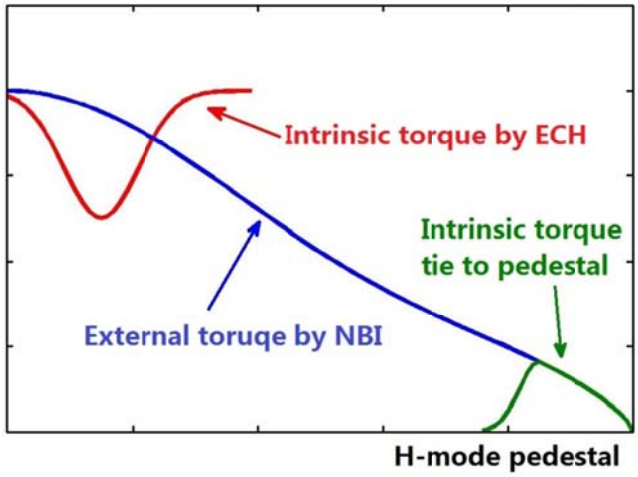

Figure 5 Cartoon showing three torques for ECH+NBI H-mode plasma

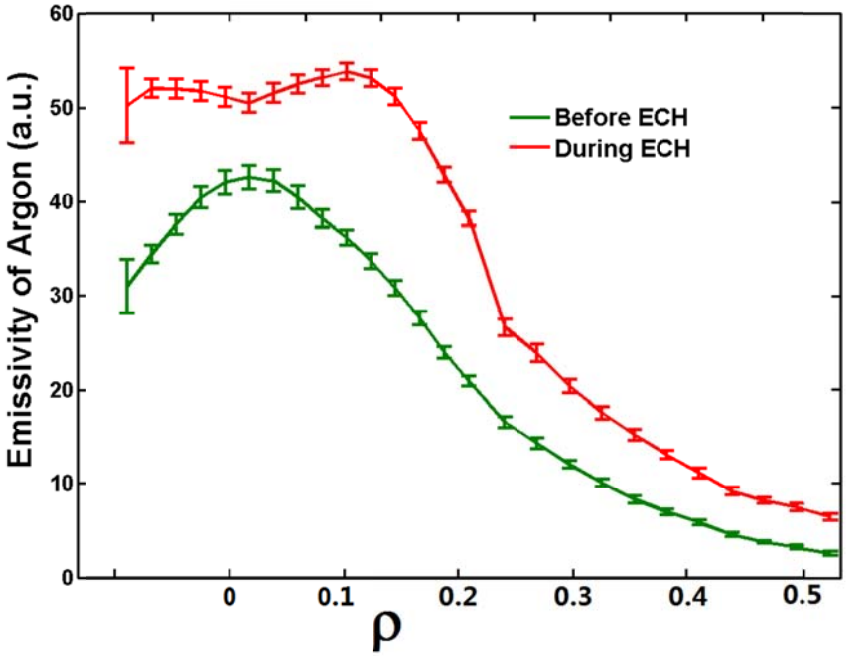

Figure 6 The emissivity profiles of helium-like argon.

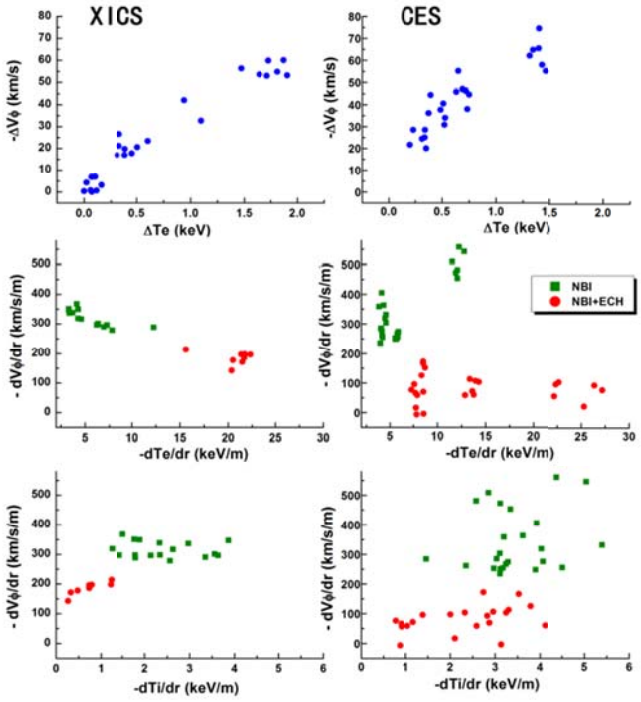

Figure7. The correlation between ΔV_ϕ and ΔTe (top), ∇V_ϕ and ∇Te (middle), ∇V_ϕ and ∇Ti (bottom). The data in XICS panel is focused on the very core region (ρ~0.2) and cover the full ECH injection period and some time before and after ECH. CES data is come from several positions (ρ from 0.2 to 0.54) and several time points

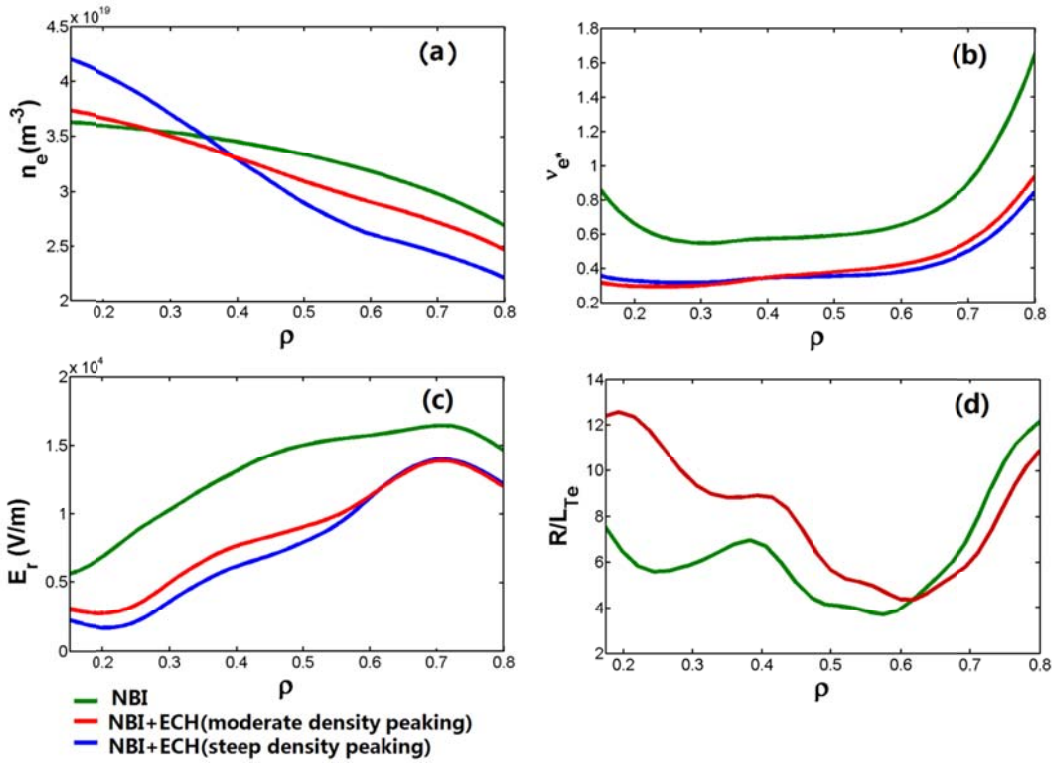

Figure8 (a) synthetic density profile, (b) effective collision frequency, (c)E×B shearing rate, (d) normalized inverse gradient scale length of T_e

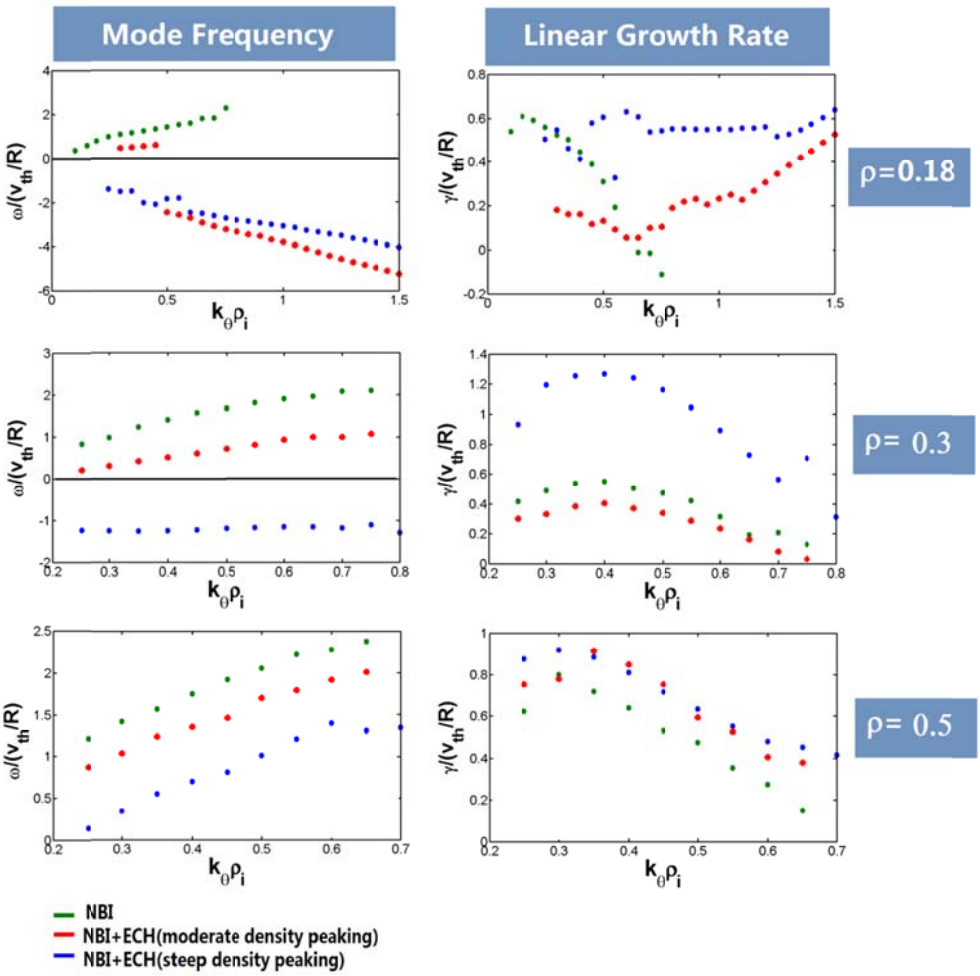

Figure9. Mode frequency and linear growth rate simulated with GS2 at three positions ((ρ=0.18, 0.3, and 0.5).

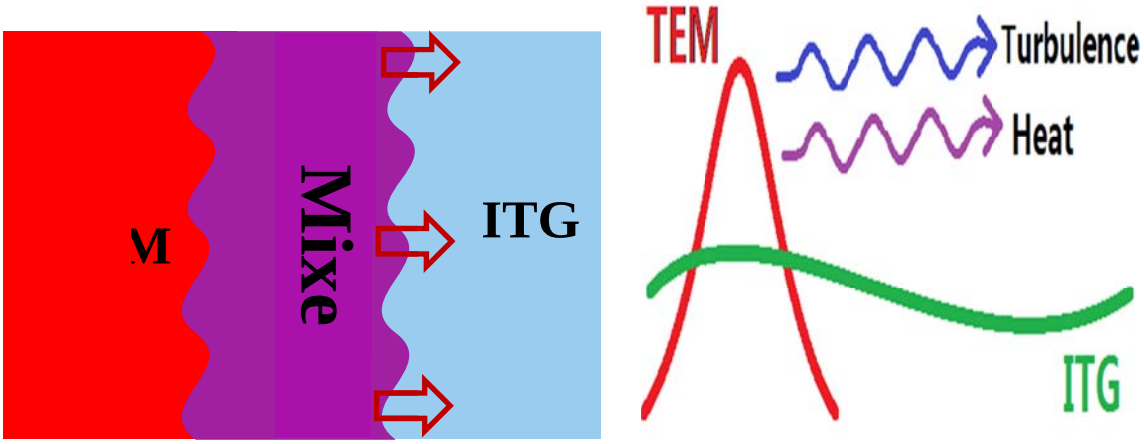

Figure 10. cartoons showing the mixed states(left) and extension of TEM influence with nonlinear processes (right)